Decomposition of NO_x with Low-Temperature Plasmas at Atmospheric Pressure: Neat and in the Presence of Oxidants, Reductants, Water, and Carbon Dioxide

Jian Luo,[†] Steven L. Suib,*[,†,‡] Manuel Marquez,[†,§] Yuji Hayashi,[||] and Hiroshige Matsumoto[⊥]

U-60, Department of Chemistry, University of Connecticut, Storrs, Connecticut 06269-4060, Department of Chemical Engineering and Institute of Materials Science, and Department of Electrical Engineering and Applied Physics, Yale University, New Haven, Connecticut 06511, Fujitsu Laboratories, Ltd., 1015 Kamikodanaka, Nakahara 211 Japan, and Department of Chemistry, Nagasaki University, Bunkyomachi 1-14 Nagasaki 852 Japan

Received: April 27, 1998; In Final Form: July 29, 1998

The fundamental aspects of decomposition of NO with atmospheric pressure low-temperature plasmas have been systematically investigated in this study. A charge-coupled device detector has been employed to record the emission spectra of plasma-induced reactions for mechanistic analyses. Specific energy consumption for the process (kilojoules per mole of converted NO) has been defined and discussed in detail. Variables such as initial NO concentrations ($[NO]_0$), space velocities, and input voltages are all important in decomposition of NO using plasmas. Additives such as O_2, carbon, CO, CO_2, water vapor, and hydrocarbons also produce significant effects. Effective direct decomposition of NO_x of 250−10000 ppm has been achieved using novel all-quartz tubular plasma reactors, which show good activity and excellent stability, especially in the presence of water. The relatively lower initial activity and very good stability with all-glass reactors relative to metal-electrode reactors (which deactivate markedly) suggest that NO decomposition with plasmas in quartz reactors is noncatalytic while catalytic effects are involved with metal-electrode reactors. In addition, the all-quartz reactors have much higher energy efficiency for NO_x decomposition than metal reactors. The kinetic equation of NO_x decomposition can be expressed as $-d[NO_x]/dt = k[NO_x]^{1/4}$ for a 1% NO/He system. An Arrhenius correlation has been established between the rate constant k and the measured voltage during plasma reaction. The addition of CO, ethane, or carbon species considerably increases the conversion of NO by reducing NO_x into CO_x and N_2. The conversion of NO_x may be enhanced by the addition of O_2 and is inhibited by the presence of water vapor or CO_2. Conversion of NO_x decreased on increasing the concentration of H_2O or CO_2. A mechanism based on the interaction between excited species of carrier gas and NO (comprising the participation of radicals such as N·, O·, ·OH, and H·) has been proposed on the basis of emission spectroscopic data.

I. Introduction

During the past decade the removal of NO_x has become a central scientific concern[1−5] because of its key role in many global environmental problems such as acid rain, photochemical smog formation, and the Greenhouse effect. Current measures for NO_x removal include the catalytic reduction of NO_x and direct decomposition of NO_x. The former requires reductants such as ammonia and hydrocarbons to react with NO_x. Some difficult technological efforts are required to add external reductants, as in the SCR (selective catalytic reduction) process or to use extra gasoline to maintain a reducing atmosphere in such systems.[2,3,6] The direct decomposition of NO_x into nitrogen and oxygen can avoid the drawbacks of current methods of NO_x removal. As a result, increasing attention has been paid to the direct decomposition of NO_x in the presence of oxygen owing to economic considerations and technical simplicity.[12−14]

Many types of catalysts have been tested for NO_x removal. Among these catalysts metal-modified zeolites such as Cu−ZSM-5 and Co−ZSM-5 have been extensively examined.[7,12−14,17−22] Modified Fe−ZSM-5 was recently reported[19,36] to be tolerant to steaming conditions; however, almost all the currently tested catalysts suffer from such problems as easy catalyst deactivation, poor thermal and hydrothermal stability, and unsatisfactory activity.

Plasmas may provide an alternative approach for NO_x removal. Plasma technologies have been applied to destroy atmospheric pollutants, such as CFC's.[23−26] The removal of SO_x and NO_x in flue gases using radio-frequency, microwave, electron beam, or barrier discharge plasmas in the presence of reductants such as NH_3 and oil were also reported.[27−32,38−40] However, few studies have yet been published on the basic kinetics and mechanisms for decomposition of NO_x in plasmas. In these published studies, metal electrodes in plasma reactors may also act as catalysts, which makes distinguishing the role of the effects of plasmas and catalysis by metal electrodes very difficult.

Optical emission spectroscopy (OES) has been widely used in studies of material processing with plasmas owing to convenience in monitoring excited species in a plasma system.

* To whom correspondence should be addressed.
[†] University of Connecticut.
[‡] Department of Chemical Engineering and Institute of Materials Science, Yale University.
[§] Department of Electrical Engineering and Applied Physics, Yale University.
[||] Fujitsu Laboratories.
[⊥] Nagasaki University.

S1089-5639(98)02013-1 CCC: $15.00
Published on Web 09/17/1998

A charge-coupled device (CCD) detector has very high sensitivity and very low noise, which makes it ideal for detection of excited species of different concentrations in plasmas and direct monitoring of the chemical processes that occur during NO decomposition with plasmas.

In the past few years, deNO_x processes for simulated exhaust and flue gases using different types of low-temperature plasma reactors have been studied by us. We report here the fundamental kinetic and mechanistic features of NO_x decomposition (mainly using NO/He as reactants) with systematic studies of NO_x decomposition in all-quartz plasma reactors, in which metal electrodes are not present. These model reactions involve a He diluent. We have carried out other experiments in air with the addition of water and CO_2, simulating air-rich exhaust gas and flue gas conditions, and have found similar trends. A rate equation for NO_x decomposition has been obtained, with a correlation between the rate constant and input voltage. The dependence of NO decomposition on input voltages (or energy), space velocities, the presence of additives, and concentrations of NO was studied in detail. The results were compared with some metal-electrode plasma reactors, where catalytic effects of metal-electrode surfaces have been observed. Interactions between excited helium species and NO have been investigated to obtain mechanistic information.

In addition to the direct decomposition of NO_x, considerable research is now focused on the removal of NO_x using reductants such as hydrocarbons, alcohols, CO, H_2, and carbonaceous species over various catalysts.[7,8,14,34] The effects of reductants such as predeposited carbon, ethane, and CO on NO_x decomposition in plasmas have been examined here. NO_x is generated in flue gases from power plants and as exhaust from motor vehicles, always with the coproduction of high concentrations of water and CO_2. Therefore, effects of additions of water vapor, oxygen, and carbon oxides on conversion of NO_x have also been investigated.

II. Experimental Section

A. Reactors, Electrical Circuits, and Apparatus. A tubular type all-glass reactor and several metal-electrode reactors were used in this research. A basic tubular reactor consists of a stainless steel rod coated with a specific metal cathode (8.0 mm i.d.) and an encircling glass tube (9.5 mm i.d.), which is wrapped with aluminum foil (60 mm wide), which serves as an anode. Reactants flow through the gap between the glass tubing and the metal rod, which could also act as a catalyst during reactions. In an all-glass tubular reactor a copper rod of 7 mm is inserted into glass tubing (8.0 mm external diameter) and only acts as an electrode. The reactant does not contact any metal part in this reactor, and it is therefore referred to as an all-glass tubular reactor.

An electrical circuit diagram is shown in Figure 1. High voltage necessary for producing plasmas is provided by an uHV-10 ac (alternative current, 8.1 kHz) power supply. The reactor and resistors are connected as shown in the electrical circuit diagram. The voltage of the reactor during reactions is determined using a high-voltage probe. The corresponding current is determined using a 100 Ω resistor and a low-voltage probe. Current and voltage measurements of the reactor during reactions are recorded from their waveforms and monitored with a DL-1540 Yokogawa Oscilloscope.

B. Reactant Preparation and Analyses of Reaction Products. Certified standard gas mixtures of nitric oxide (1.0% and 0.45% NO in He, 1.0% NO in N_2) were obtained from MG Industries Gas Products. Gases of 10% O_2 in He, 10% CO_2 in He, 5% CO in He, and ethane were from Connecticut Airgas, Inc. Mixtures of different compositions and concentrations were prepared from the above-mentioned gases using a gas mixing panel.

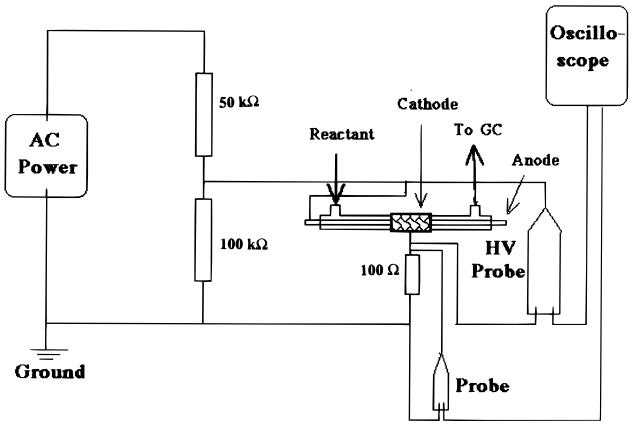

Figure 1. Diagram of the electric circuit of the plasma reactor and related apparatus.

Water vapor concentrations of 1.3%, 3.2%, 5.2%, and 12.3% were introduced into the reactor by using He to flow through a bubbler containing water. For concentrations of 5.2% and 12.3% the bubbler, lines, and reactor were placed in an isotemp oven set at 50 °C so that water vapor will not condense in the lines or reactor. The downstream gas was condensed by an ice-cold trap to remove most of the water vapor before GC analysis.

Analyses of N_2, O_2, NO, CO, CO_2, and H_2O are done on-line with an HP-5990 A GC (gas chromatograph) equipped with a TCD (thermal conductivity detector), an HP 3395 integrator, and a 25 ft packed Carboxcen 1000 column, using He as GC carrier gas for the analyses of oxygen, nitrogen, nitric oxide, carbon monoxide, and carbon dioxide, whose concentrations are determined by external standard calibration methods. Relative errors for these GC analyses are within 5%. Two GC runs are needed for each analysis. For the analyses of oxygen and nitrogen, column temperatures of 60 °C and head pressures of 30 psi were used. For the analyses of NO, CO, and CO_2, a combination of 120 °C and 40 psi was employed.

An MKS-UTI PPT Quadrupole Residual Gas Analyzer Mass Spectrometer system (with a Faraday Cup detector and a variable high-pressure manifold) was used to detect nitrogen oxides such as nitrogen dioxide (NO_2), nitrous oxide (N_2O), dinitrogen trioxide (N_2O_3), and dinitrogen tetraoxide (N_2O_4), as well as HNO_2, HNO_3, and O_3. Since quantitation using a quadrupole MS is not very accurate, the concentrations of NO_2 have been obtained from calculations (eq 10).

C. Optical Emission Spectroscopic Studies of NO Decomposition. Emission spectra of the plasmas were obtained in the range of 200−900 nm with a 270 M Spex liquid nitrogen-cooled CCD detector. Helium of ultrahigh purity (99.999%) was used first to determine the excitation temperature of plasmas at different input voltages. Reactants of NO of different concentrations and additives were then used for studies of plasma-induced reactions. Experimental setups and reaction conditions are identical to those described above except that several holes (2 mm in diameter) are made in the aluminum foil to allow light from plasmas to be collected and directed to the monochromator through a fiber optic with a microscope objective lens. Relative errors in determining peak areas are within 2%. Excitation temperatures of plasmas (which are close to electron temperatures for near-atmospheric pressure plasmas)

TABLE 1: Variation of Electrical Parameters and Rate Constants for NO_x Decomposition with Input Voltage Using an All-Glass Tubular Plasma Reactor[a]

V_{in} (kV)	V_p (kV)	V_p' (kV)	I_p (mA)	P (W)	P' (W)	T_{exc} (K)	k ($mol^{3/4}$ $L^{-3/4}$ s^{-1})
1.75	1.38	0.46	17.3	0.696	0.232	3600	$1.47 \times 10-4$
2.25	1.83	0.67	13.2	1.20	0.439	3700	$2.40 \times 10-4$
2.75	2.38	0.93	12.8	2.03	0.794		$3.52 \times 10-4$
3.25	2.85	1.20	12.8	2.94	1.238	4600	$4.23 \times 10-4$
3.75	3.30	1.17	18.6	4.50	1.67	5100	$7.55 \times 10-4$
4.25	4.02	1.11	34.1	7.66	2.11	5300	$14.8 \times 10-4$

[a] V_{in}, input voltage; V_p, peak voltage; I_p, peak current; P, power; V_p', plasma peak voltage; P', plasma power.

are obtained from a Boltzmann plotting method from the He emission lines as described in ref 9.

D. Definitions and Calculations. The peak voltage (V_p) and current (I_p), root-mean-square voltage (V_{rms}), current (I_{rms}), and power (P) read from the waveforms are parameters for both the reactor and plasma. The power and voltage is further corrected for the reaction (referred to as plasma voltage and plasma power, V' and P', respectively) after measuring the impedance of the quartz reactor. Energy consumption levels for the reaction (specific energy consumption, usually given as kilojoule per mole of converted NO) are thus obtained. These data are more conveniently shown as electronvolt per converted NO molecule as given in eq 1.

$E(1)$:

$$1 \text{ kJ/mol NO} = (1000/96\,487) \text{ eV/NO} = 0.0104 \text{ eV/NO} \quad (1)$$

where the Faraday constant, 96487 C/mol of electrons was used. Another specific energy consumption, $E(2)$, which is in terms of N_2 produced, is also used (kilojoule per $^1/_2$ mole produced N_2). Only the energy consumption in the reactor was considered because this represents energy needed in chemical reactions. The energy consumption of the HV-10 power supply is an ancillary energy requirement and can be optimized by proper design of electronic components. The input voltage is referred to as a lower voltage if it is not higher than 3.25 kV. Data of P', V', I_{rms}, and V_{rms} at different input voltages are listed in Table 1.

The volume of the plasma region (V_{red}, 1.24 mL, as calculated from the length of aluminum foil, the interior diameter of the outer glass tube, and the diameter of the inner glass tube or metal electrode) is defined as plasma space or reaction space. Residence time (t_{red}) is defined as the retention period (in seconds) of gas mixtures in the plasma space and is obtained from eq 2

$$t_{red} = 60V_{red}/F = 74.4/F \quad (2)$$

where F is the flow rate of the gas mixture (in mL/min). The gas hourly space velocity (GHSV, h^{-1}) for a reaction is obtained from eq 3:

$$\text{GHSV} = 60F/V_{red} = 48.4F \quad (3)$$

Conversions of NO (χ) are calculated from the concentrations of NO before ($[NO]_0$) and after ([NO]) reaction as given by eq 4:

$$\chi, \% = (1 - [NO]/[NO]_0) \times 100\% \quad (4)$$

In the plasma reaction NO_2 is also produced and decomposed, especially when O_2 is added into the reactant. The definition of total NO_x decomposition is given in eq 5:

$$\chi', \% = (1 - 2[N_2]/[NO]_0) \times 100\% \quad (5)$$

Total NO_x decomposition is a more important parameter for NO_x conversion since it reflects the degree of direct decomposition of NO into N_2/O_2. The conversion of NO may lead to the partial formation of NO_2, which is also toxic.

Concentrations of products were obtained by GC analysis except those of NO_2 ($[NO_2]$), which were calculated from the conversion of NO and the concentration of N_2 ($[N_2]$) as given below in eq 10. Since N_2, O_2, NO, and NO_2 are related by eqs 7−9, only two of the concentrations are independent ($[N_2]$ and [NO] are chosen). In addition to the form of vol %, the concentration is also presented as mol/L as given in eq 6 (the reaction was done at 22 °C):

$$\text{conc., mol/L} = \text{vol \%} ((1000 \text{ mL/L}) \times (273 \text{ K}/295 \text{ K}) \times (1 \text{ mol}/22\,400 \text{ mL}) \quad (6)$$

III. Results

A. Variation of Plasma Parameters with Input Voltages. In the all-quartz reactor, plasmas are generated at a minimum input voltage of 1.60 kV. Experiments of NO decomposition started at 1.75 kV. When input voltage increases, the peak voltage, peak current, and discharge time all increase. The plasma peak voltage, however, increases first as the input voltage is increased to 3.25 kV, above which it begins to decrease. The plasma peak voltage, current, and plasma power at different input voltages are listed in Table 1. These plasma parameters are mainly controlled by adjusting the input voltage, changing little even with additions of H_2O, O_2 or air, CO_2, CO, and C_2H_6 in the ranges of concentration employed in this study. As shown in Table 1, the ratio of plasma power (P') to the total power of both the reactor and plasma (P) decreases as the input voltage increases, when the density of charged particles (and therefore the current) increases, leading to less impedance of the plasma.

The excitation temperatures (T_{exc}) of plasmas calculated from the Boltzmann plotting method[9] are shown in Table 1. The temperature increases from 3600 to 5300 K when the input voltage is increased from 1.75 to 4.25 kV. A thermometer was placed on the aluminum foil, showing that the temperature is below 35 °C at all voltages. Thermocouples placed in the reactor under a He flow indicate a maximum temperature after 2 h of about 70 °C. This result indicates that the reactions here are not thermal reactions induced by high gas temperatures.

B. Decomposition of NO/He in All-Quartz Reactors. *1. Dependence of NO Conversion on Input Voltages and Residence Times.* The variations of NO conversion and concentration of N_2 formed with residence time at different input voltages for 1% NO in He are shown in Figures 2 and 3, respectively. The conversion increases as the input voltage and/or residence time increases. High conversions of NO of over 90% at 3.75 kV and t_{red} can be maintained for at least 3 days, showing good stability of the all-quartz reactor for NO decomposition.

The variation of selectivity to NO_2 with residence time at different input voltages is shown in Figure 4. At low conversions the main products are N_2, O_2, and NO_2, indicating that the main reactions at this stage are NO decomposition into N_2/O_2 and NO_2 formation from NO reacting with O_2. As the conversion increases with increasing residence time, the concentrations of N_2 and O_2 increase while NO_2 concentration increases first and then decreases. This indicates that at high conversion (longer retention time) the decomposition of NO and the formation and decomposition of NO_2 are the main reactions.

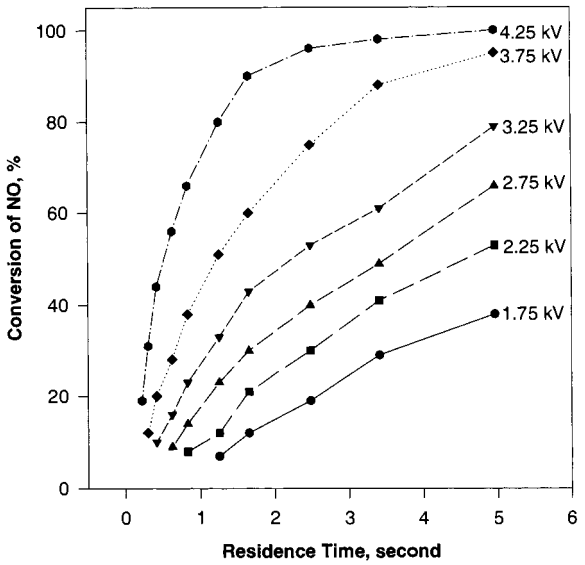

Figure 2. Variation of NO conversion with residence time at different input voltages.

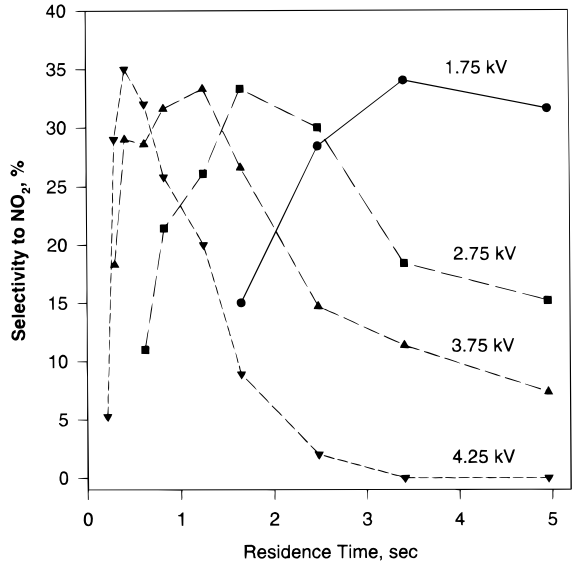

Figure 4. Dependence of selectivity to NO_2 on residence time at different input voltages.

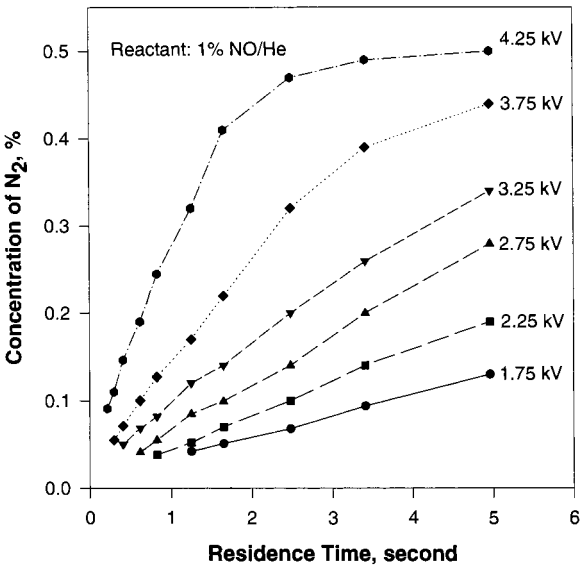

Figure 3. Variation of concentration of N_2 formed with residence time at different input voltages.

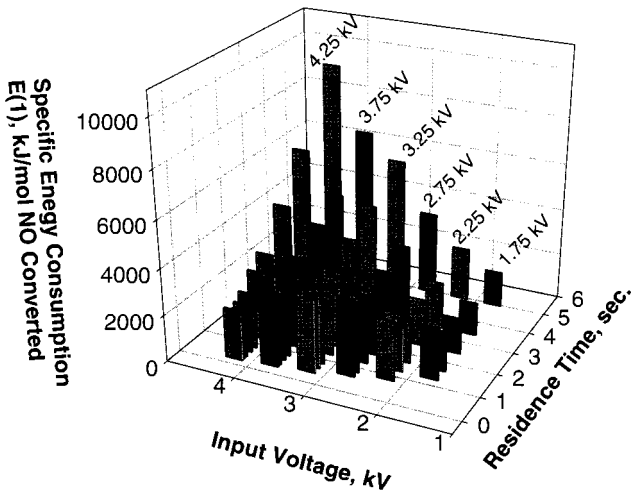

Figure 5. Variation of specific energy consumption with respect to NO conversion ($E(1)$) with input voltages and residence times.

The selectivity to NO_2 reaches a maximum (ca. 30%) at different residence times which decreases with increasing input voltage. Effective conversion of both NO and NO_2 can be achieved at high voltages and longer residence times.

A quadrupole MS was used to detect products at trace levels. When plasmas were generated, very low concentrations (<10−12 mmHg) of N_2O_3 ($m/z = 76$), N_2O_4 ($m/z = 92$), and low concentrations (<0.01%) of N_2O (m/z of 30 and 44) and O_3 ($m/z = 48$) were observed. The signal of N_2O might be overlapped by CO_2 ($m/z = 44$). These nitrogen oxide species might be intermediates in NO decomposition.

2. Variation of Specific Energy Consumption with Input Voltages and Residence Time. The specific energy consumption, an indication of the energy efficiency for the decomposition of NO with plasmas, varies with both the input voltage and residence time. At all input voltages, the specific energy consumption in terms of NO conversion ($E(1)$) decreases first, reaches a minimum, and then increases as the residence time is increased (Figure 5). For a given GHSV, the energy consumption usually exhibits a maximum at 2.75−3.25 kV. For 1% NO in He, the energy consumption is usually in the range of 1400−4000 kJ/mol converted NO. This can exceed 5000 kJ/mol NO (ca. 50 eV/NO) at high input voltages and short residence times.

With only a few exceptions, the specific energy consumption in terms of N_2 formed ($E(2)$) increases on decreasing GHSV and is usually 2−10 eV/NO larger than the corresponding specific energy cost in terms of NO conversion. This specific energy also exhibits a maximum at 2.75−3.25 kV for a GHSV > 1700 h^{-1}. At longer residence times the energy consumption increases sharply and continuously as the input voltage increases (Figure 6).

In general, $E(2)$ is greater than the corresponding $E(1)$. The difference between the two energy consumption values is found to be proportional to the selectivity to NO_2. For a given input voltage, $E(1)$ exhibits a minimum at the residence time when S_{NO_2} is highest. The decrease in $E(1)$ is due to oxidation of some NO to NO_2 by O_2 that is initially produced.

C. Comparison between All-Quartz and Metal Reactors. Results of NO decomposition with tubular metal plasma reactors with rhodium and iron as electrodes are shown in Figure 7. Much higher initial NO conversions are obtained with both metal electrodes with respect to the all-quartz reactor, suggesting that

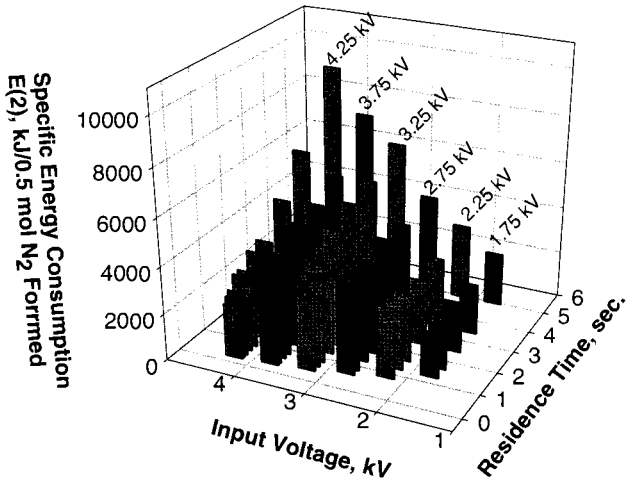

Figure 6. Variation of specific energy consumption with respect to N_2 from decomposition ($E(2)$) with input voltages and residence times.

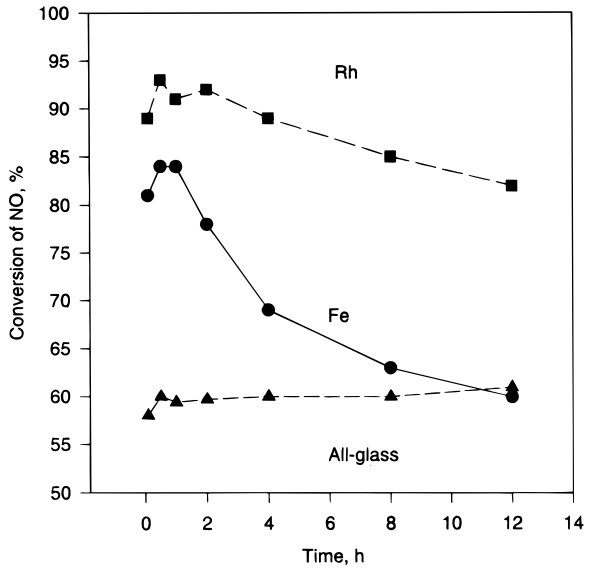

Figure 7. Variation of NO conversion with time-on-stream with Rh, Fe, and all-quartz tubular reactors (input voltage, 3.25 kV; GHSV, 2000 h^{-1}).

metal surfaces can catalyze the decomposition of NO. Considerable deactivation was observed with both metal-electrode reactors. At 3.25 kV and a GHSV of 2000 h^{-1}, NO conversion decreased from 85% at $t = 30$ min to 47% at $t = 12$ h in an iron tubular reactor. After reaction, the surface of the iron electrode became dark and rough. The deactivation of the metal-electrode reactor is due to changes of the metal surface (oxidized to metal oxides). Although the Rh reactor is much more stable than the Fe reactor, the activity of the Rh decreased to 53% at $t = 60$ h. The Rh electrode became much duller after reaction. Under the same conditions, an all-quartz reactor maintains an NO conversion of ca. 60% with almost no deactivation. The quartz surface of the all-quartz reactor did not change, even after reaction at much higher voltages for much longer time. This very stable surface may account for the very stable activity of the all-quartz reactor. The relatively lower initial activity and very good stability suggest that the decomposition of NO in plasmas in an all-quartz reactor may be noncatalytic while catalysis is involved with metal-electrode reactors, whose initial activity is higher but decreases in time.

Another advantage of the all-quartz reactor is its much higher energy efficiency for NO decomposition than that for metal reactors. Under our experimental conditions the specific energy consumption for NO decomposition in an all-quartz reactor is ca. 2.3×10^3 kJ/mol NO (ca. 23 eV/NO), less than $^1/_6$ that of metal reactors with Rh or Fe as electrodes. The specific energy consumption for an all-quartz reactor is much smaller than that for a similar deNO_x process using a corona plasma reactor, which is 200−1000 eV/NO.[42]

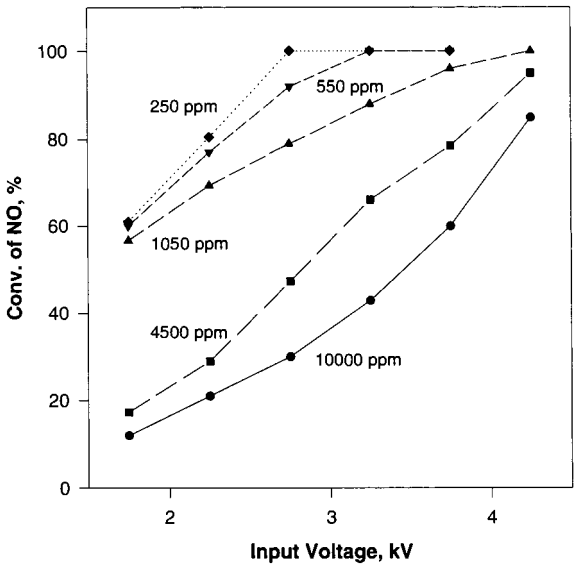

Figure 8. Variation of NO conversion with concentration of NO.

D. Effects of $[NO]_0$ on NO Conversion, Selectivity to NO_2 and Specific Energy Consumption. Reactions of NO of different concentrations were studied using a fixed GHSV of 3000 h^{-1} at different voltages (Figure 8). As the concentration decreases, NO conversion increases sharply. Complete decomposition of NO is obtained at $[NO]_0 = 1050$ ppm, higher input voltages (3.25 kV and higher), and GHSV of 3000 h^{-1} or lower. For a reactant $[NO]_0$ of 250 ppm, a 100% conversion of NO was achieved at 2.25 kV and GHSV of 3000 h^{-1}.

The production of NO_2 is greatly reduced at lower $[NO]_0$. The maximum selectivity to NO_2 decreases from over 35% at $[NO]_0 = 10\,000$ ppm to 10% at $[NO]_0 = 1050$ ppm. Selectivity further decreases to less than 5% at $[NO]_0 = 550$ ppm. Almost no NO_2 can be detected in reactions of $[NO]_0$ of 250 ppm.

The specific energy consumption for a 1% NO in He at GHSV of 3000 h^{-1} is <2300 kJ/mol NO. While the conversion of NO increases sharply on decreasing $[NO]_0$, the energy consumption increases in a similar manner, especially at high input voltages, reaching 5.7×10^4 kJ/mol NO at 3.25 kV and $[NO]_0$ of 250 ppm (1.2×10^4 kJ/mol NO at 1.75 kV). Since a conversion of NO of 100% can be easily achieved at low input voltages (<2.25 kV) for low $[NO]_0$, higher input voltages (and therefore high energy consumption) are unnecessary.

E. Reaction of NO in the Presence of Additives. Reactions discussed in this section are for a mixture of 0.45% NO in He along with additives, which is prepared from 1% NO in He and proper additives. The results are discussed as follows.

1. Effects of Addition of Reductants. Three types of reductants, predeposited carbon, carbon monoxide, and ethane, were used to test the effects of reductants on the decomposition of NO. The results are shown in Figure 9.

The addition of carbon greatly increases the conversion of NO, especially at lower input voltages. The conversion increases further as the amount of carbon increases. Both CO and CO_2 are detected as products even at low voltages. As reaction proceeds the concentrations of CO and CO_2 decrease, and the conversion of NO also decreases slowly. This suggests

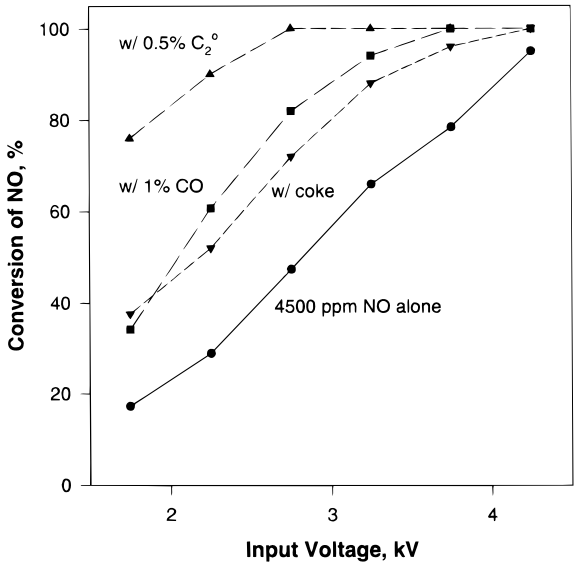

Figure 9. Conversion of NO vs input voltage showing effects of addition of carbon, CO, and C_2H_6 (4500 oom NO in He; GHSV, 2300 h^{-1}).

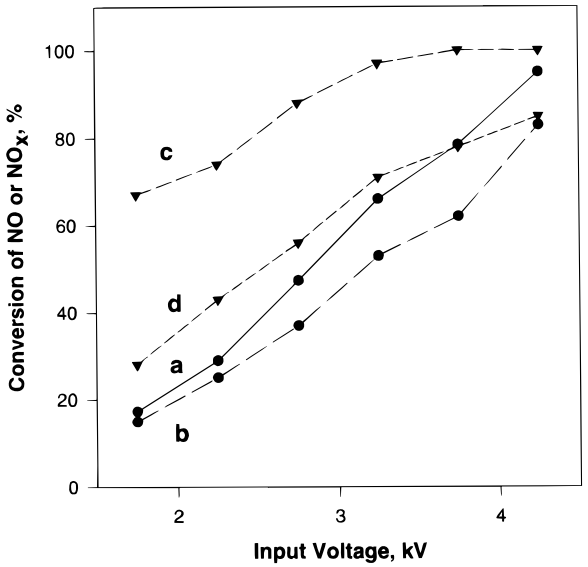

Figure 10. Conversion of NO (a and c) and total NO_x decomposition (b and d) vs input voltage showing effects of addition of 5% O_2 (GHSV, 2300 h^{-1}; and b 4500 ppm NO in He alone; c and d, 5% O_2 added).

that carbon deposits can react with NO or O_2 produced from NO, thus greatly increasing the conversion.

The addition of CO has similar effects to those of predeposited carbon, with NO decomposition being greatly enhanced. The conversion of CO itself is small at lower voltages (<10% at 2.75 kV). CO conversion becomes important only as input voltages increase over 3.25 kV, reaching ca. 40% at 3.75 kV. CO_2 appears to be the main product from CO. No carbon deposits were observed after the reaction was stopped.

The addition of ethane greatly enhances NO conversion. As shown in Figure 9, ethane is the most efficient reductant that we studied that increased the conversion of NO. However, several hydrocarbon species other than ethane are produced besides CO and CO_2, such as methane, ethene, acetylene, and many higher hydrocarbons. The conversion of ethane is <30% even at 4.25 kV.

2. Effects of Addition of O_2 on NO_x Decomposition. When oxygen is added to the reactant, some NO is oxidized to NO_2, whose concentration depends on both [NO] and [O_2]. The reactants are actually a mixture of NO and NO_2 (NO_x). For $[NO_x]_0$ of 4500 ppm, the fraction of NO_2 in the feed increases sharply as [O_2] in the feed increases (being over 50% when [O_2] > 1.2%). At lower $[NO_x]_0$ (1050 ppm or less), the fraction of NO_2 is less than 25% even at [O_2] of 10%.

At $[NO_x]_0 = 4500$ ppm, the conversion of NO increases greatly as oxygen is added, although a large fraction (up to 60%) of NO goes to NO_2. The total NO_x decomposition is also higher than that without addition of oxygen (Figure 10) (except at [O_2] of over 5% and higher input voltages), showing that the addition of oxygen favors the decomposition of total NO_x in this voltage range. At higher [O_2] and higher voltages, however, the total NO_x decomposition is slightly less than that without added oxygen.

At $[NO_x] = 1050$ ppm, the conversions of both NO and total NO_x decrease with oxygen added at [O_2] < 3%. At higher [O_2], the conversion of NO increases slightly at lower input voltages (2.75 kV or less) but decreases considerably at higher voltages. The total NO_x decomposition always decreases with added oxygen under all conditions that were employed.

3. Effects of Addition of Water and CO_2. When the concentration of water is small (1.3%), the conversion of NO changes slightly at lower input voltages but decreases considerably at higher voltages. Conversion of NO decreases greatly as the concentration of water vapor in the reactant is further increased to 3.2%, especially at higher voltages (Figure 11). At $[H_2O] = 12.3\%$, the conversion of NO is less than half that of the water-free decomposition of NO at all input voltages, dropping to only 38.1% even at 4.25 kV and a GHSV of 3000 h^{-1}.

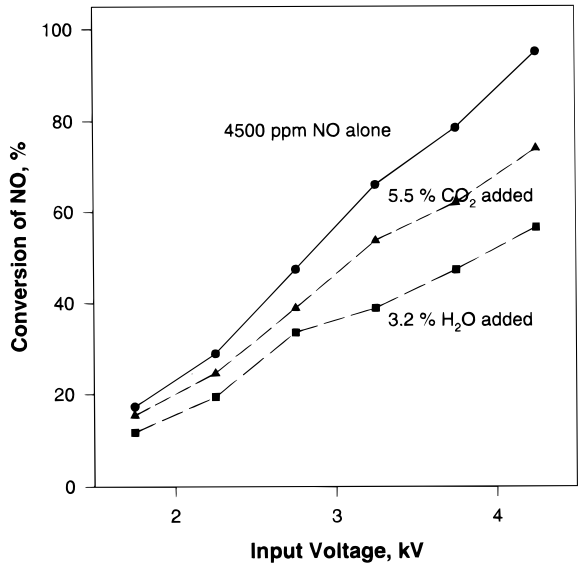

Figure 11. Conversion of NO showing effects of addition of H_2O and CO_2 (4500 ppm NO in He; GHSV, 2300 h^{-1}).

The conversion of NO was considerably decreased by addition of CO_2 (5.5% in the mixture, Figure 11), especially at higher voltages and was further decreased when [CO_2] was increased. The concentration of CO_2 shows almost no change at lower input voltages but slightly decreases at higher voltages, with considerable amounts of CO detected, showing that the decomposition of CO_2 into CO and O_2 competes with NO decomposition. However, the conversion of CO_2 is less than 9.0% even at 4.25 kV.

As mentioned above, the presence of additives caused little change in the required power of the plasma yet resulted in considerable changes in conversion. The specific energy

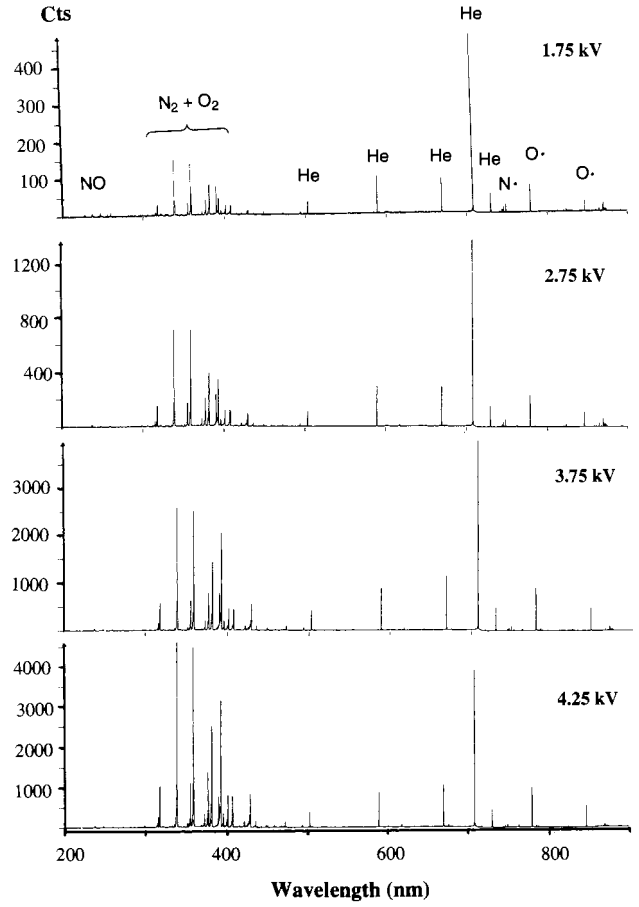

Figure 12. Optical emission spectra of 1% NO in He at different input voltages.

consumption, therefore, changes accordingly with change in NO conversion. No detectable concentrations of HNO_2, HNO_3, or H_2O_2 were observed with quadrupole MS when H_2O was added. The partial pressure of O_3 did not show a marked increase ($<10-12$ Torr) when O_2 is added. These species probably adsorb in the reaction lines and decompose before being detected by the MS system.

F. Optical Emission Spectroscopic Studies of NO Decomposition by CCD Detector. *1. Spectroscopic Studies of Conversion of NO in He.* Figure 12 shows the emission spectra of plasmas of 1% NO in He at various input voltages. At low input voltage and short residence time (1.6 kV and 0.4 s for NO conversion < 2%) emission of NO (237 nm), N((747 nm), O((777 nm), and N_2/O_2 were observed as well as emissions for various He species. When input voltages increased, the intensity of excited helium species (He, He^+, etc.), those of excited radicals such as N· and O·, and those of excited N_2 and O_2 all increased, along with a decrease in relative intensities of NO emission lines. When the residence time increased, similar trends were observed for NO, N_2, and O_2. The relative intensities of radicals of N· and O· increased first, reached a maximum, and then decreased. This clearly indicates that NO decomposes to N_2 and O_2 with radicals of N· and O· as intermediates.

Spectra were also taken along the axis of the reactor. The intensities of He emission change slightly, but those of N· and O· change considerably. Oscillations of the relative intensities of N_2, O_2, and NO as well as radicals of N· and O· can be observed along the axis (Figure 13). This suggests that oscillatory reactions of NO along the reactor axis exist in the plasma region. This oscillation can be observed at various GHSV. Note that O· oscillations may not be so obvious because the data are been normalized to the most intense He emission (700 nm). Inhomogeneity of the plasma along the axis or interactions between plasma species may account for the oscillation of the relative species.

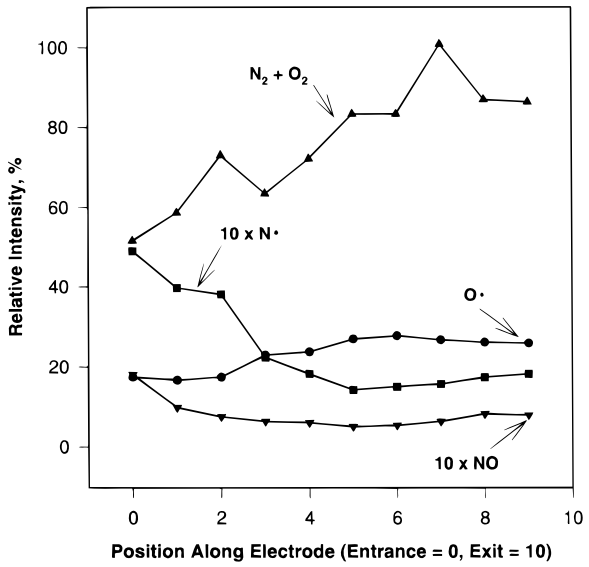

Figure 13. Variation of relative emission intensities (relative to emission line of He at 700 nm) along the axis of the all-quartz plasma reactor.

2. Studies of Effects of Additives via Optical Emission. When O_2 of <1% was added to the reactant, the emission spectra did not change much except that O_2 and O· species increased considerably. The He species decreased in intensity as $[O_2]$ increased, almost disappearing when the $[O_2]$ was over 5%. The addition of air has similar effects to those of O_2.

The intensities of N·, O·, and N_2/O_2 decreased sharply when water vapor was added to the 1% NO/He reactant even at $[H_2O]$ of 0.4%. HO radicals with emissions at ca. 310 nm were observed. Radicals of O· were also observable; however, the intensities were much smaller than those of H_2O-free systems (Figure 14). When CO_2 was added instead of H_2O, species of CO, CO_2, and CO_2^+ were observed, with a marked decrease in intensities of the He series as compared to the NO/He-only reactant, although the CO_2-induced decrease was not as effective as that of H_2O.

Minor additives of CO or C_2H_6 (ca. 0.4% each) also led to considerable decrease in the intensities of He emission, and additional emission of CO (287 nm) and CO_2 (485 nm) are observed. Additional CH· radicals (430 nm) and CO, CO_2 are observed when C_2H_6 is used. Meanwhile, the emission of O· radicals decreased. A mixture of (0.45% NO, 5% O_2, 5% CO_2, and 3.2% H_2O) in He or a mixture of similar composition with N_2 in place of He showed, only emission of oxygen, nitrogen, and ·OH.

IV. Discussion

A. Kinetics Studies of NO Decomposition. From results in section IV.A, some model reactions in the all-glass reactor with 1% NO are those described in eqs 7−9:

$$NO \rightarrow {}^1/_2N_2 + {}^1/_2O_2 \quad (7)$$

$$NO + {}^1/_2O_2 \rightarrow NO_2 \quad (8)$$

$$NO_2 \rightarrow {}^1/_2N_2 + O_2 \quad (9)$$

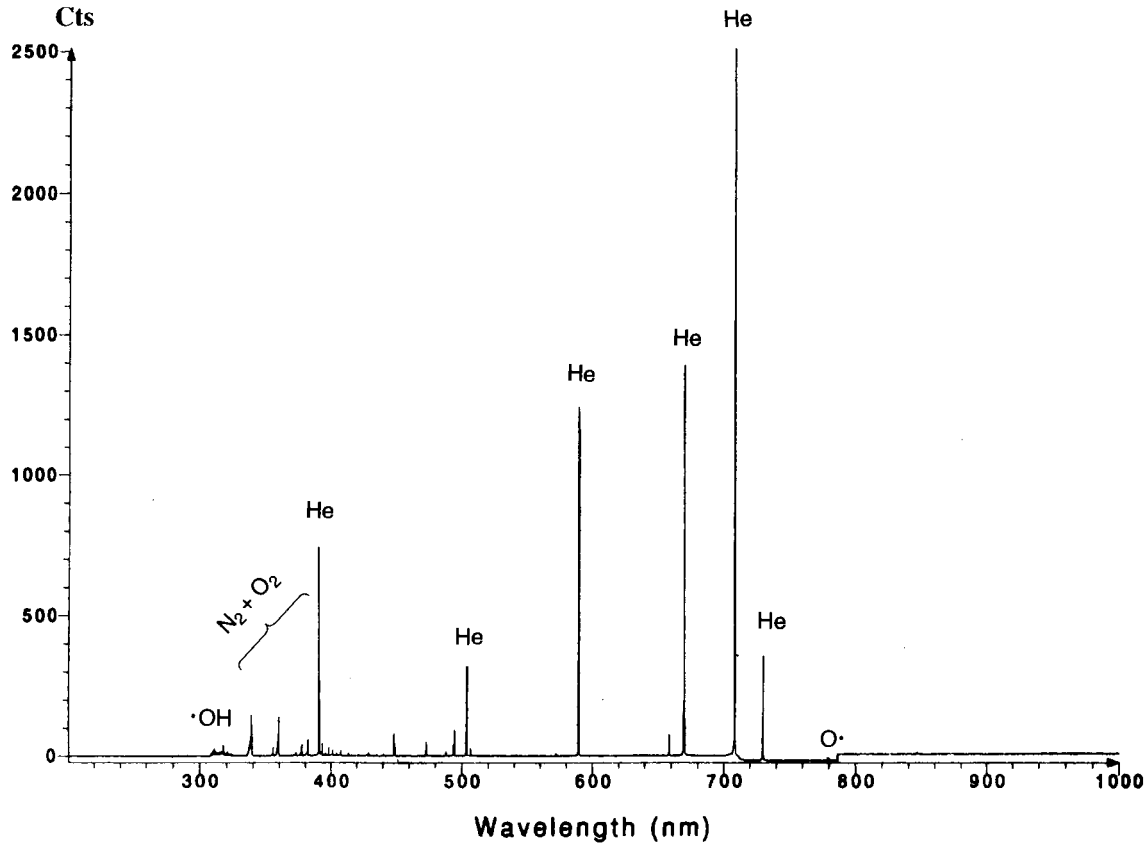

Figure 14. Optical emission spectrum of reaction of 0.45% NO in He with addition of 3.2% H_2O at 3.75 kV and GHSV of 2300 h^{-1}.

Since the amounts of nitrogen species other than NO, NO_2, and N_2 are negligible, a nitrogen balance can be obtained from eq 10:

$$[NO] + 2[N_2] + [NO_2] = [NO]_0 \quad (10)$$

Two equations (eqs 11 and 12) can be derived from eq 10:

$$[NO_2] = [NO]_0 - [NO] - 2[N_2] = \chi[NO]_0 - 2[N_2] \quad (11)$$

$$[NO] + [NO_2] = [NO_x] = [NO]_0 - 2[N_2] \quad (12)$$

At shorter residence times $[N_2]$ and $[NO_2]$ increase linearly with increasing residence times. At higher conversions, the concentration of NO_2 decreases with increasing residence time. These data suggest that at low conversions the major reactions are eqs 7 and 8. At high conversions (>50%) reactions 7−9 may all be important.

The reaction of a mixture of 2% N_2 + 2% O_2 in He using an all-glass plasma reactor was also carried out. No detectable amounts of NO_x were observed under conditions employed for NO_x decomposition. This indicates that the reverse reaction for NO_x decomposition is not important. A simplified reaction scheme for NO_x decomposition and a kinetic expression are given in eqs 13 and 14, respectively (k is the NO_x decomposition rate constant):

$$NO_x \rightarrow {}^1/_2N_2 + {}^x/_2O_2 \quad (13)$$

$$-d[NO_x]/dt = k[NO_x]^n \quad (14)$$

where NO and NO_2 are summed as total reactant, NO_x. A similar approach for simplifying the reaction system was employed in kinetic studies of many important petrochemical processes such as catalytic cracking of gas oil.[41] From the reaction rates of NO of different concentrations (10 000, 4500, and 1050 ppm), the reaction order of NO_x decomposition is found to be 0.28, which for simplification leads to a reaction order of $n = {}^1/_4$. The corresponding differential kinetic equation for NO_x decomposition is given in eq 15:

$$d[NO_x]/dt = k[NO_x]^{1/4} \quad (15)$$

A $[NO_x]$ versus time (t) formula is thus obtained by integrating eq 14, as given in eq 16:

$$[NO]_0^{3/4} - [NO_x]^{3/4} = {}^3/_4kt \quad (16)$$

Substituting eq 11 into eq 15 leads to a relationship between the rate of decomposition of NO_x and the rate of formation of N_2, as given in eq 17

$$[NO]_0^{3/4} - (1 - 2[N_2])^{3/4} = {}^3/_4kt \quad (17)$$

with which the rate constants at different input voltages are obtained from linear regressions with $[N_2]$ data of Figure 3. The rate constant (listed in Table 1) increases exponentially as the input voltage increases, very similar to the variation of rate constants of conventional reactions with reaction temperatures.

B. Mechanistic Description of NO_x Decomposition in Plasmas. The results of section IV.A show that peak voltage and peak current remain relatively constant when NO or other additives are present in the plasma system. The properties of the plasma are mainly determined by the carrier gas at a given input voltage. The interaction between high-temperature electrons and He carrier gas (instead of reactant NO) is the main initial energy transfer in the plasma. This may be justified considering that the carrier gas is the predominant component

in the system. As shown in Table 2, the excitation temperature of the plasma decreases markedly when NO and/or the additives are presented, showing energy transfer between excited He species and reactant molecules, which are activated by excited carrier gas species and further undergo decomposition. CCD studies show that NO decomposes to N_2/O_2 via N·/O· intermediates. On the basis of these results, a simple mechanism for the decomposition of NO can be proposed as shown in eqs 18−26 that represent model reactions

$$e^- + A \rightarrow A^E \quad (18)$$

$$NO + A^E \rightarrow NO^* \quad (19)$$

$$NO^* \rightarrow N\cdot + O\cdot \quad (20)$$

$$2N\cdot \rightarrow N_2 \quad (21)$$

$$2O\cdot \rightarrow O_2 \quad (22)$$

$$NO + O\cdot \rightarrow NO_2 \quad (23)$$

$$NO + N\cdot \rightarrow N_2O \quad (24)$$

$$NO + {}^1/_2O_2 \rightarrow NO_2 \quad (25)$$

$$NO_2 + A^E \rightarrow NO^* + O\cdot \quad (26)$$

where A^E represents an active species that can activate the reactants. These are high-energy state carrier gas molecules or ions that are excited by high-temperature electrons (e^-) in plasmas. The starred species (NO*) are activated species. When H_2O is added, plasma-induced radicals of HO· and H· may participate in the reaction. Similarly, corresponding plasma-induced species will participate when CO_2, O_2, C, CO, C_2H_6, and air are added.

The concentration of N_2O is very small at all residence times in this system. Reaction 24 can be neglected. Reaction 23 is also believed to be a minor pathway. The formation of NO_2 should be mainly due to eq 25, a nonplasma reaction between NO and molecular oxygen. At lower $[NO]_0$ and therefore low $[O_2]$, the formation of NO_2 becomes insignificant.

As mentioned in section IV.B, the difference in the two types of specific energy consumption is proportional to the selectivity to NO_2, which suggests that the reaction of NO with oxygen to NO_2 does not need energy from the plasma. Reaction 25 is not plasma-induced, which is confirmed by the fact that a fraction of NO is oxidized to NO_2 by externally added oxygen without the presence of a plasma.

The peak current of the plasmas increases as input voltage is increased. More electrons with higher energy and therefore more excited active species in the plasma are present that can lead to a higher conversion of NO. The number of active species is limited so that the conversion of NO is decreased when the concentration of NO is increased.

C. Effects of Addition of Reductants and O_2, CO_2, and Water. CO_2 and water are always produced with the formation of NO_x in power plants and motor vehicles in the presence of oxygen. Many studies suggest that the presence of water is detrimental to catalysts, especially to zeolite-based catalysts, owing to steam-induced dealumination at elevated temperatures.[14,35] The conversion of NO was also affected by the addition of O_2 and/or CO_2 to different degrees.

The addition of molecules other than NO and the inert carrier gas could scavenge active species in the plasma, leading to a decrease in intensities of He emission and a decrease in the conversion of NO. This explains the decrease in activity when CO_2 and water are present in the reaction. Considerable amounts of carbon monoxide were detected at higher voltages when CO_2 was added. Similarly, H_2 of very low concentration was detected when water was added. This indicates that reactions of the additives may compete with NO_x decomposition in the plasma. The consequence of the presence of competing reactants is that fewer molecules of NO_x may likely be activated, thus leading to a decrease in the conversion of NO_x. Although activity is reduced when water is added, the very important aspect of the all-quartz plasma reactor is that the conversion of NO_x is very stable. In comparison, almost all zeolite-based catalysts suffer from severe deactivation owing to dealumination by steaming with the presence of water vapor at elevated temperatures.[35] Metal-electrode plasma reactors also deactivate rapidly owing to deterioriation of the electrode surface in the presence of NO_x and H_2O in plasmas.

Some NO is oxidized to NO_2 when O_2 is added into the reactant. In reactions with plasmas, the decomposition of NO_2 is easier than that of NO. The addition of O_2 can lead to an increase in NO conversion and total NO_x conversion at lower input voltages. However, oxygen is one of the products of NO_x decomposition, whose presence will increase the rate of the reverse reaction (NO_x syntheses). In addition, oxygen could also act as a scavenger or at least a competitive species. Such oxygen species at higher input voltages will hinder the conversion of NO_x. At low initial [NO], only a small fraction of NO is converted to NO_2 in the presence of O_2, when inhibiting effects of O_2 prevail.

Reductants, however, can reduce NO in plasmas. For instance, carbon can react with NO to form CO and CO_2, as shown in eq 27

$$C + NO \rightarrow CO_x + N_2 \quad (27)$$

Carbon may also react with oxygen atoms formed from the breakdown of NO (as indicated by the reduction of intensities of O· emission), thus greatly facilitating the conversion of NO. The enhancement of NO_x conversion by carbonaceous species with plasmas may find important applications in diesel engine vehicles, which need simultaneous removal of both carbonaceous particles and NO_x.[34] CO and hydrocarbons have similar effects. Some intermediate species, such as radicals of CH_x· (as observed in this work) and C_xH_y·,[44] are formed in plasmas when C_2H_6 or other hydrocarbons are used as a reductant. These species may produce stronger reducing power than carbon and CO leading to selective reduction of NO_x.

Similar results have been observed for the reaction of NO in N_2 and simulated flue gases and exhaust gases, except that the minimum input voltages for generating plasmas in these systems are much higher than in the NO/He system.

V. Conclusions

Effective decomposition of NO_x of different concentrations (250−10000 ppm) can be achieved with very good stability using an all-quartz tubular plasma reactor. NO_x decomposition in plasmas in an all-quartz reactor is noncatalytic and much more energy efficient than that in metal reactors. Input voltages, space velocities, NO_x concentrations, and the presence of other species all play an important role in the conversion of NO_x. Higher conversions can be obtained at higher input voltages, smaller space velocities, and smaller initial concentrations of NO. Addition of CO_2 or water inhibits the conversion of NO_x.

The presence of reductants such as carbon, CO, and hydrocarbons enhances the conversion of NO. The addition of O_2 can facilitate NO_x conversion at higher $[NO]_0$ and lower input voltages but decrease NO_x conversion at lower $[NO]_0$. The all-quartz reactor is very stable in the presence of water vapor and O_2 and shows good activity in NO_x decomposition. In the plasma system, energy transfer occurs initially from electrons to the carrier gas, whose excited species further transfer energy to reactant molecules and additive molecules that undergo activation and decomposition. The decomposition of NO_x into N_2 and O_2 with plasmas proceeds via N· and O· radicals. Oscillations in the plasma have been observed. In addition, two types of reactions are observed in the process including plasma-induced reactions, such as the activation and decomposition of NO_x into N_2/O_2, and nonplasma reactions, such as the reaction of NO with produced O_2 to form NO_2.

Acknowledgment. The authors thank Dr. K. Yin, Dr. S. Brock, Mr. X. Chen, and Mr. J. Rozak for helpful discussions and assistance in experiments. Support for this research from Fujitsu Limited, Hokushin Corporation, and Honda R. and D. Co. is gratefully acknowledged.

References and Notes

(1) Manahan, S. *Environmental Chemistry*, 6th ed.; Lewis Publishers: Boca Raton, FL, 1994; pp 338−346.
(2) Armor, J. N. *Appl. Catal. B* **1992**, *1*, 221−256.
(3) Cusmano, J. A. *CHEMTECH* **1992**, *22*, 482−489.
(4) Jacoby, M. *Chem Eng. News* **1997**, *75* (June 30), 32−35.
(5) Taylor, K. C. *Catal. Rev.-Sci. Eng.* **1993**, *35*, 457−481.
(6) Shelef, M.; Graham, G. M. *Catal. Rev.-Sci. Eng.* **1994**, *36*, 433−457.
(7) Marquez-Alvarez, C.; Rodriguez-Ramos, I.; Guerrero-Ruiz, A.; Haller, G. L.; Fernandez-Garcia, M. *J. Am. Chem. Soc.* **1997**, *119*, 2905−2914.
(8) Miyazaki, T.; Nagasaka, S.; Kamiya, Y. *J. Phys. Chem.* **1993**, *97*, 10715−10719.
(9) Hasegawa, T.; Umemoto, M.; Haraguchi, H.; Hsiech C.; Montaser, A. In *Inductively Coupled Plasmas in Analytical Atomic Spectroscopy*; Montaser, A., Golightly, D. W., Eds.; VCH Publishers: New York, 1992; p 375.
(10) Miyazaki, T.; Nagasaka, S.; Kamiya, Y. *J. Am. Chem. Soc.* **1994**, *116*.
(11) Anderson, L. C.; Xu, M.; Mooney, C. E.; Rosynek, M. P.; Lunsford, J. H. *J. Am. Chem. Soc.* **1993**, *115*, 6322−6326.
(12) Iwamoto, M.; Furukawa, H.; Mine, Y.; Uemura, F.; Mikuriya, S.; Kagawa, S. *J. Chem. Soc., Chem. Commun.* **1986**, 1272−1273.
(13) Iwamoto, M.; Yahiro, H. *Catal. Today* **1994**, *22*, 5−18.
(14) Armor, J. N. *Catal. Today* **1995**, *26*, 99−105.
(15) Corma, A.; Fornes, V.; Palomares, E. *Appl. Catal. B* **1997**, *11*, 233−242.
(16) Li, Y.; Armor, J. N. *J. Catal.* **1994**, *145*, 1−9.
(17) Sarkany, J.; Sachtler, W. M. H. *Zeolites* **1994**, 14, 7−11.
(18) Petunchi, J. O.; Marcelin, G.; Hall, W. K. *J. Phys. Chem.* **1992**, *96*, 9967−9975.
(19) Feng, X.; Hall, W. K. *J. Catal.* **1997**, *166*, 368−376.
(20) Grinsted, R. A.; Jen, H.-M.; Montreuil, C. N.; Roksz, M. J.; Shelef, M. *Zeolites* **1993**, *13*, 602−606.
(21) Grunert, W.; Hayes, N.; Joyner, R.; Shpiro, E.; Siddiqui, M.; Baeva, G. *J. Phys. Chem.* **1994**, *98*, 10832−10846.
(22) Li, C.; Bethke, K. A.; Kung, H. H.; Kung, M. *J. Chem. Soc., Chem. Commun.* **1995**, 813−814.
(23) Futamura, S.; Yamamoto, T. *IEEE Trans. Ind. Appl.* **1997**, *33*, 447−453.
(24) Evans, D.; Rosocha, L. A.; Anderson, G. K.; Coogan, J. J.; Kushner, M. J. *J. Appl. Phys.* **1993**, *74*, 5378−5386.
(25) Hsiao, M. C.; Merritt, B. T.; Penetrante, B. M.; Vogtlin, G. E.; Wallman, P. H. *J. Appl. Phys.* **1995**, *78*, 3451−3456.
(26) Penetrante, B. M.; Hsiao, M. C.; Bardsley, J. N.; Merritt, B. T.; Vogtlin, G. E.; Wallman, P. H.; Kuthi, A.; Burkhart, C. P.; Bayless, J. R. *Phys. Lett. A* **1995**, *209* (Dec), 69−77.
(27) Chang, M. B.; Cheng, C. F. *Sci. Total. Environ.* **1997**, *198*, 73−78.
(28) Gallinberti, I. *Pure Appl. Chem.* **1988**, *60*, 663−674.
(29) Chang, M. B.; Balbach, J. H. *J. Appl. Phys.* **1991**, *69*, 4409−4417.
(30) Murakami, N.; Yamakawa, T.; Murata, M.; Nishida, S.; Konda, T. JP 02203920, 1990.
(31) Birckigt, R. Ger. Offen. DE 19534950, 1997.
(32) Deng, G.; Zhang, Y.; Yu, Y.; Zou, D.; Hou, H.; Li, C. *J. Environ. Sci.* **1997**, *9*, 11−19.
(33) Eremin, E. N.; Mat'tsev, A. N.; Belova, V. M. Russ. *J. Phys. Chem.* **1971**, *45*, 635−638.
(34) Li, W.; Sirilumpen, M.; Yang, R. T. *Appl. Catal. B* **1997**, *11*, 347−363.
(35) Li, Y.; Armor, J. N. *J. Catal.* **1994**, *150*, 376−387.
(36) Jacoby, M. *Chem Eng. News* **1997**, *75* (Sept 15), 8−9.
(37) Boenig, H. V. *Plasma Science and Technol.*; Cornell University Press: Ithaca, NY, 1982; pp 32−34.
(38) Civitano, L.; Sani, E. In *Plasma Technology*; Capitelli, M., Gorse, C., Eds.; Plenum Press: New York, 1992; pp 153−166.
(39) Clements, J. S.; Mizuno, A.; Finney, W. C.; Davis, R. H. *IEEE Trans. Ind. Appl.* **1989**, *25*, 62−69.
(40) Fujii, K. In *Plasma Technology*; Capitelli, M., Gorse, C., Eds.; Plenum Press: New York, 1992; pp 143−152.
(41) Nace, D. M.; Viltz, S. E.; Weekman, V. W. *Ind. Eng. Chem., Proc. Des. Dev.* **1971**, *10*, 530−538.
(42) Tas, M. A.; Hardeveld, R. van; Veldhuizen, E. M. van; *Plasma Chem. Plasma Process.* **1997**, *17*, 371−391.
(43) Pearse, R. W. B.; Gaydon, A. G. The Identification of Molecular Spectra; Chapman and Hall: New York, 1976.
(44) Onoe, K.; Fujie, A.; Yamaguchi, T.; Hatano, Y. *Fuel* **1997**, *76*, 281−281.